JACS
JOURNAL OF THE AMERICAN CHEMICAL SOCIETY

ARTICLE

pubs.acs.org/JACS

The Shape of the $Sc_2(\mu_2\text{-}S)$ Unit Trapped in C_{82}: Crystallographic, Computational, and Electrochemical Studies of the Isomers, $Sc_2(\mu_2\text{-}S)@C_s(6)\text{-}C_{82}$ and $Sc_2(\mu_2\text{-}S)@C_{3v}(8)\text{-}C_{82}$

Brandon Q. Mercado,[†] Ning Chen,[‡] Antonio Rodríguez-Fortea,[§] Mary A. Mackey,[∥] Steven Stevenson,[∥] Luis Echegoyen,[*,‡] Josep M. Poblet,[*,§] Marilyn M. Olmstead,[*,†] and Alan L. Balch[*,†]

[†]Department of Chemistry, University of California, One Shields Avenue, Davis, California 95616, United States

[‡]Department of Chemistry, University of Texas at El Paso, El Paso, Texas 79968, United States

[§]Departament de Química Física i Inorgànica, Universitat Rovira i Virgili, c/Marcel-lí Domingo s/n, 43007 Tarragona, Spain

[∥]Department of Chemistry, University of Southern Mississippi, Hattiesburg, Mississippi 39406, United States

Supporting Information

ABSTRACT: Single-crystal X-ray diffraction studies of $Sc_2(\mu_2\text{-}S)@C_s(6)\text{-}C_{82}\cdot Ni^{II}(OEP)\cdot 2C_6H_6$ and $Sc_2(\mu_2\text{-}S)@C_{3v}(8)\text{-}C_{82}\cdot Ni^{II}(OEP)\cdot 2C_6H_6$ reveal that both contain fully ordered fullerene cages. The crystallographic data for $Sc_2(\mu_2\text{-}S)@C_s(6)\text{-}C_{82}\cdot Ni^{II}(OEP)\cdot 2C_6H_6$ show two remarkable features: the presence of two slightly different cage sites and a fully ordered molecule $Sc_2(\mu_2\text{-}S)@C_s(6)\text{-}C_{82}$ in one of these sites. The Sc−S−Sc angles in $Sc_2(\mu_2\text{-}S)@C_s(6)\text{-}C_{82}$ (113.84(3)°) and $Sc_2(\mu_2\text{-}S)@C_{3v}(8)\text{-}C_{82}$ differ (97.34(13)°). This is the first case where the nature and structure of the fullerene cage isomer exerts a demonstrable effect on the geometry of the cluster contained within. Computational studies have shown that, among the nine isomers that follow the isolated pentagon rule for C_{82}, the cage stability changes markedly between 0 and 250 K, but the $C_s(6)\text{-}C_{82}$ cage is preferred at temperatures ≥250 °C when using the energies obtained with the free encapsulated model (FEM). However, the $C_{3v}(8)\text{-}C_{82}$ cage is preferred at temperatures ≥250 °C using the energies obtained by rigid rotor−harmonic oscillator (RRHO) approximation. These results corroborate the fact that both cages are observed and likely to trap the $Sc_2(\mu_2\text{-}S)$ cluster, whereas earlier FEM and RRHO calculations predicted only the $C_s(6)\text{-}C_{82}$ cage is likely to trap the $Sc_2(\mu_2\text{-}O)$ cluster. We also compare the recently published electrochemistry of the sulfide-containing $Sc_2(\mu_2\text{-}S)@C_s(6)\text{-}C_{82}$ to that of corresponding oxide-containing $Sc_2(\mu_2\text{-}O)@C_s(6)\text{-}C_{82}$.

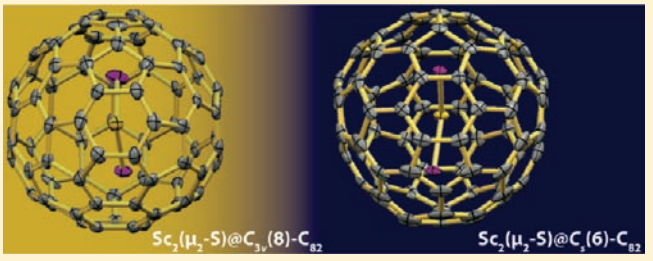

INTRODUCTION

The year 1985 marked the seminal fullerene publication that proposed the icosahedral structure of C_{60}.[1] Additionally in that year, Smalley et al. reported the first example of an endohedral fullerene: La@C_{60}.[2] Numerous advances have since been made in the preparation and isolation of fullerenes and endohedral fullerenes.[3−5] Endohedrals have attracted attention as potential medical imaging agents and optoelectronic devices.[6,7] Including nonmetallic atoms as starting materials in the synthesis of fullerenes provides one avenue to increase the scope of chemical entities incorporated inside a fullerene.[8] Thus, atoms of groups 14, 15, and 16 have been trapped inside fullerenes to form various clusters by incorporating a variety of nonmetallic atoms in gaseous and solid form into the fullerene generation process.[7,9] Stevenson et al. first reported the detection and structural elucidation of the trimetallic nitride (TN) fullerene $Sc_3N@I_h\text{-}C_{80}$.[10] In this case, N_2 is responsible for producing the nitride anion. Endohedral fullerenes, containing the M_3N group have been made with scandium, yttrium, and every lanthanide, (excluding promethium, europium, samarium, and ytterbium) with cage sizes ranging from C_{68} to C_{96}.[11,12] The formation of $Sc_3CH@I_h(7)\text{-}C_{80}$,[13] $Sc_xC_2@I_h(7)\text{-}C_{80}$ (x = 3, 4),[14,15] $Sc_2C_2@C_{2v}(6073)\text{-}C_{68}$,[16] $Sc_2C_2@C_{3v}(8)\text{-}C_{82}$,[17] $Sc_2C_2@D_{2d}(23)\text{-}C_{84}$,[18] and $Gd_2C_2@D_3(85)\text{-}C_{92}$[19] as stable compounds demonstrates the versatility of carbon as an encapsulated atom. Recently, both nitrogen and carbon have been detected at the center of a related molecule, $Sc_3CN@I_h(7)\text{-}C_{80}$.[20]

Oxygen with a μ_3 or μ_2 bonding motif is also observed in clusterfullerenes. A face-capped tetrahedron of scandium ions in $Sc_4(\mu_3\text{-}O)_2@I_h\text{-}C_{80}$ was the first example of an oxygen-containing clusterfullerene.[21,22] This class of oxometallic fullerenes includes the largest cluster isolated to date: the seven-atom unit in $Sc_4(\mu_3\text{-}O)_3@I_h\text{-}C_{80}$.[23] We recently reported the isolation and characterization of $Sc_2(\mu_2\text{-}O)@C_s(6)\text{-}C_{82}$, a third member of oxometallic fullerenes. There are nine isomers of a C_{82} cage

Received: January 12, 2011
Published: April 07, 2011

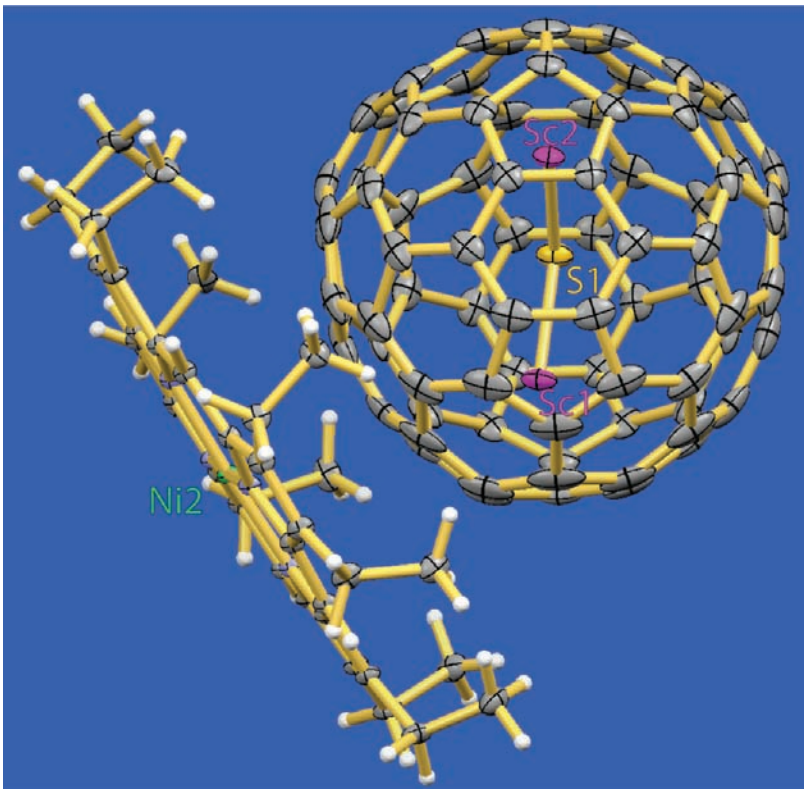

Figure 1. Fully ordered endohedral fullerene at site A in $Sc_2(\mu_2\text{-}S)@C_s(6)\text{-}C_{82}\cdot Ni^{II}(OEP)\cdot 2C_6H_6$. All non-hydrogen atoms shown are depicted with 50% thermal contours. The mirror plane of the fullerene is oriented vertically perpendicular to the plane of the page. For clarity, the benzene molecules have been omitted.

(three C_2 isomers, three C_s isomers, two C_{3v} isomers, and one C_{2v} isomer) that follow the isolated pentagon rule.[24] While computations indicated that the $C_{3v}(8)\text{-}C_{82}$ cage would be the lowest energy isomer of $Sc_2(\mu_2\text{-}O)@C_{82}$ at low temperatures, the $C_s(6)\text{-}C_{82}$ isomer was predicted to be the lowest energy cage when considering temperatures greater than 1200 K. This represented the first example in which the relevance of the thermal and entropic contributions to the stability of the fullerene isomer has been clearly confirmed through the characterization of the X-ray crystal structure.[25]

In addition to oxygen, sulfur has also been detected in new endohedrals with the formula $M_2S@C_{2n}$, comprising a second species of clusterfullerenes containing group 16 atoms. The sulfide was suspected to be a bridging atom similar to the oxide in $Sc_2(\mu_2\text{-}O)@C_s(6)\text{-}C_{82}$. Dunsch and co-workers first reported the formation of a sulfide clusterfullerene using a graphite rod doped with solid guanidinium thiocyanate and scandium oxide.[26] One sulfide endohedral was isolated by HPLC and identified as $Sc_2S@C_{3v}(8)\text{-}C_{82}$ by UV−vis and IR spectroscopy coupled with DFT calculations. Echegoyen et al. reported the isolation of two isomers of $Sc_2S@C_{82}$ via the addition of gaseous SO_2 into a modified Krätschmer−Huffman generator.[27] Their report included the assignment of the cage isomers, utilizing UV−vis spectroscopy and electrochemistry to distinguish the $C_{3v}(8)$ isomer from a previously undetected $C_s(6)$ isomer. Here, we report the first X-ray structures of both $Sc_2(\mu_2\text{-}S)@C_s(6)\text{-}C_{82}$ and $Sc_2(\mu_2\text{-}S)@C_{3v}(8)\text{-}C_{82}$. We also performed calculations that account for thermodynamic and entropic effects, as performed on $Sc_2(\mu_2\text{-}O)@C_s(6)\text{-}C_{82}$, along with related electrochemistry and computational studies involving the stabilities of these compounds.

RESULTS

Crystallographic Studies. Crystals for both $Sc_2(\mu_2\text{-}S)@C_s(6)\text{-}C_{82}\cdot Ni^{II}(OEP)\cdot 2C_6H_6$ and $Sc_2(\mu_2\text{-}S)@C_{3v}(8)\text{-}C_{82}\cdot Ni^{II}(OEP)\cdot 2C_6H_6$ were obtained by slow diffusion of a benzene solution of $Ni^{II}(OEP)$ into a benzene solution of the purified endohedral, followed by gradual evaporation until the samples were nearly dry. Both crystals contain fully ordered fullerene cages.

The asymmetric unit in $Sc_2(\mu_2\text{-}S)@C_s(6)\text{-}C_{82}\cdot Ni^{II}(OEP)\cdot 2C_6H_6$ contains two fullerene sites, A and B, as well as two porphyrin sites and four benzene molecules. The crystallographic data clearly indicates that both C_{82} cages in sites A and B are $C_s(6)$ and *ordered* in this endohedral, allowing us to definitively report bond distances and angles (see Supporting Information (SI)). Remarkably, we found that one fullerene site also possesses a *completely ordered* $Sc_2(\mu_2\text{-}S)$ *unit*. Figure 1 depicts site A, the fully ordered $Sc_2(\mu_2\text{-}S)@C_s(6)\text{-}C_{82}$, and its relationship to the adjacent nickel porphyrin. The noncrystallographic mirror plane of the C_{82} cage is perpendicular to the plane of the page. Site B has only minimal disorder in the $Sc_2(\mu_2\text{-}S)$ group. This disorder was modeled with two orientations, whose occupancies refined to 0.826(2)/0.174(2). Figure 2 compares the fully ordered $Sc_2(\mu_2\text{-}S)@C_s(6)\text{-}C_{82}$ molecule in site A with the internally disordered molecule in site B.

Figure 3 shows the environments of sites A and B in $Sc_2(\mu_2\text{-}S)@C_s(6)\text{-}C_{82}\cdot Ni^{II}(OEP)\cdot 2C_6H_6$. Several aspects of the crystal structure verify the occurrence of $Z' = 2$ (i.e., the presence of two different porphyrin and fullerene sites) in this structure. In the asymmetric unit, as shown in Figure 3, each fullerene cage, at sites A and B, is embraced by the eight ethyl arms of a different

dx.doi.org/10.1021/ja200289w | J. Am. Chem. Soc. 2011, 133, 6752–6760

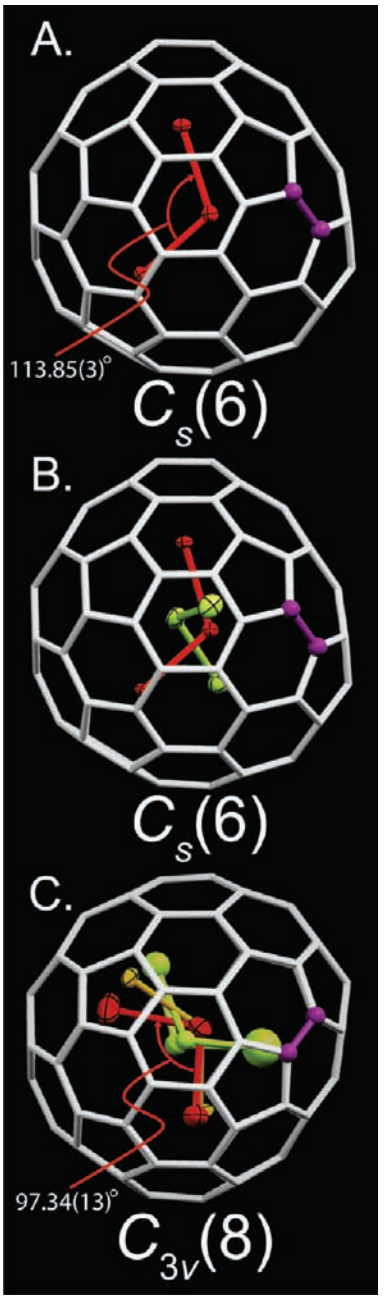

Figure 2. The two $Sc_2(\mu_2\text{-}S)@C_{82}$ isomers arranged with their mirror planes parallel to the page. Movement of the carbon atoms shown in purple could interconvert $C_s(6)\text{-}C_{82}$ and $C_{3v}(8)\text{-}C_{82}$ and may be involved in a Stone−Wales transformation between these two isomers. (A) The internally ordered fullerene site A in the asymmetric unit of $Sc_2(\mu_2\text{-}S)@C_s(6)\text{-}C_{82}\cdot Ni^{II}(OEP)\cdot 2C_6H_6$. The $Sc_2(\mu_2\text{-}S)$ unit is shown in red. (B) The internally disordered fullerene site B in $Sc_2(\mu_2\text{-}S)@C_s(6)\text{-}C_{82}$. The $Sc_2(\mu_2\text{-}S)$ unit is modeled with the major site shown in red [fractional occupancy 0.826(2)] and the minor site shown in yellow-green [fractional occupancy 0.174(2)]. (C) The internally disordered fullerene site in $Sc_2(\mu^2\text{-}S)@C_{3v}(8)\text{-}C_{82}$. The $Sc_2(\mu_2\text{-}S)$ portion is disordered and modeled in four positions. The red scandium atoms (fractional occupancy 1.20) and orange scandium atoms (fractional occupancy 0.50) share a common sulfide (fractional occupancy 0.80) shown in red. The yellow-green unit has an equally split sulfide (fractional occupancy 0.10) shared between two scandium atoms (fractional occupancy 0.30). Note the decrease in the Sc−S−Sc angle between A and C labeled in white.

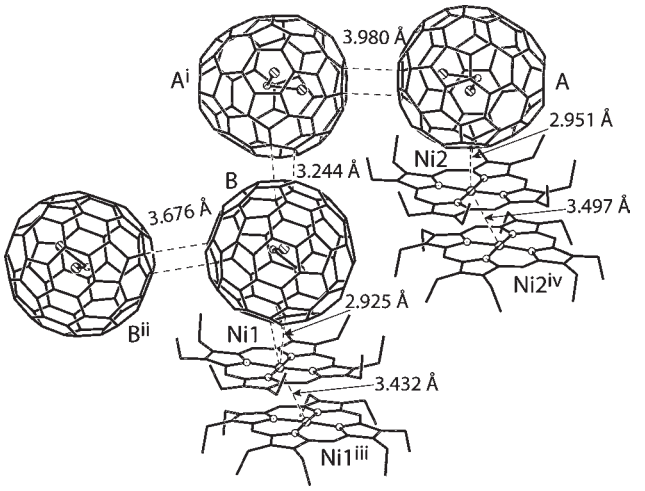

Figure 3. View of a portion of the packing of the structure of $Sc_2(\mu_2\text{-}S)@C_s(6)\text{-}C_{82}\cdot Ni^{II}(OEP)\cdot 2C_6H_6$ (benzene molecules and the second disordered Sc_2S group in ball B are omitted for clarity). This view shows inversion-related neighbors of the asymmetric unit. Symmetry codes: i = $1-x, -y, 1-z$; ii = $-x, -y, 2-z$; iii = $-x, 1-y, 2-z$; iv = $1-x, 1-y, 1-z$. The closest contacts between atoms in the nearest neighbors are shown. Standard uncertainties in distances shown are in the range 0.001−0.005 Å.

Table 1. Comparison of Bond Distances (Å) and Angles (deg) in $Sc_2(\mu_2\text{-}S)@C_s(6)\text{-}C_{82}$ and $Sc_2(\mu_2\text{-}S)@C_{3v}(8)\text{-}C_{82}$

	$Sc_2(\mu_2\text{-}S)@C_s(6)\text{-}C_{82}$		$Sc_2(\mu_2\text{-}S)@C_{3v}(8)\text{-}C_{82}$	
	exptl	theor[a]	exptl	theor[a]
		Site A		
Sc1−S1	2.3525(8)	2.34−2.37	2.335(3)[b]	2.35−2.39
Sc2−S1	2.3902(8)		2.416(4)[b]	
Sc1−S1−Sc2	113.84(3)	113.6−114.9	97.34(13)[b]	100.7−112.4
		Site B		
Sc3−S2A	2.3559(9)			
Sc4−S2A	2.3817(9)			
Sc5−S2B	2.395(6)			
Sc6−S2B	2.347(6)			
Sc3−S2A−Sc4	115.25(4)			
Sc6−S2B−Sc5	113.7(2)			

[a] Range for the four most stable orientations of the $Sc_2(\mu^2\text{-}S)$ unit inside the cage. [b] Major orientation with 0.60 fractional occupancy.

porphyrin. The porphyrins, in turn, come into close contact with an inversion-related porphyrin in a back-to-back arrangement. The Ni···Ni separation in each pair is different. In this view it is apparent that the balls at sites A and B have different rotational dispositions as well as vastly different ball-to-ball contacts to their inversion-related components. The shortest contact between the cages involves that between a ball at site A and a ball at site B.

Table 1 compares the Sc−S bond distances and Sc−S−Sc bond angles in the two sites. The parameters at both sites are similar, and indeed the orientation of the major $Sc_2(\mu_2\text{-}S)$ unit at site B is analogous to that at site A.

The pyramidalizations[28] of the fullerene carbon atoms in both sites A and B in $Sc_2(\mu_2\text{-}S)@C_s(6)\text{-}C_{82}\cdot Ni^{II}(OEP)\cdot 2C_6H_6$ are

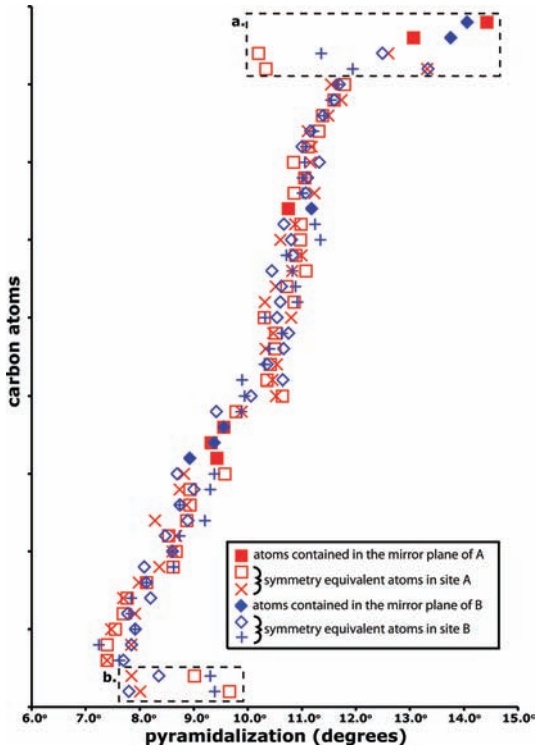

Figure 4. Pyramidalization of the symmetry-related groups of carbon atoms in the two fullerene sites of $Sc_2(\mu_2\text{-}S)@C_s(6)\text{-}C_{82}\cdot Ni^{II}(OEP)\cdot 2C_6H_6$.

shown in Figure 4. Along the vertical axis we present symmetry-related groups of carbon atoms ranked essentially from lowest pyramidalization to highest pyramidalization, with some outliers shown in dashed boxes at the bottom and top. Since each carbon cage has a mirror plane, there are 38 pairs of symmetry-related carbon atoms in the cage and six unique carbon atoms that lie in the mirror plane. Thus, there are 44 symmetry-related groups of carbon atoms plotted along the vertical axis. Since there are two fullerenes involved, there will be four carbon atoms involved in each symmetry-related group, except for the cases of carbon atoms lying on the symmetry plane, where there will be only two atoms. Those atoms that lie on the symmetry plane are identified by solid squares and diamonds. The plot shows that the pyramidalization of individual carbon atoms generally ranges from 7.5° to 11.7°. For comparison, the experimentally determined pyramidalization in C_{60} is 11.6(1)°, and the five types of carbon atoms in the D_{5h} isomer of C_{90} have pyramidalizations of 11.9(1), 12.0(1), 11.7(1), 10.4(1), 7.2(2), and 5.5(2)°.[29] The plot also shows that the agreement within a symmetry-related group is generally less than a degree, with the exception of the data enclosed in the dashed boxes. The most pyramidalized carbon atoms (those with pyramidalization >12° enclosed in box a) are the eight carbon atoms closest to the scandium atoms. Notice that their symmetry-related counterparts have much lower pyramidalizations that lie between 9.5° and 11°. Thus, the scandium atoms push the neighboring carbon atoms outward and increase their pyramidalization, an effect that has been noted previously in a very few cases.[30−32] The carbon atoms that are closest to the nickel atoms in $Ni^{II}(OEP)$ have unusually low pyramidalization compared to their symmetry-related counterparts that are further from the porphyrin as seen in the data in box b. Thus, the four carbon atoms on the left side of box b are the carbon atoms nearest the adjacent nickel atom, while the four carbon atoms on the left side are much farther from the nickel atom.

Figure 5 shows the structure of the second isomer, $Sc_2(\mu_2\text{-}S)@C_{3v}(8)\text{-}C_{82}$, and its relationship to the nickel porphyrin in $Sc_2(\mu_2\text{-}S)@C_{3v}(8)\text{-}C_{82}\cdot Ni^{II}(OEP)\cdot 2C_6H_6$. In this figure the three-fold rotation axis of the C_{82} cage lies perpendicular to the picture plane. As we observed with $Sc_2(\mu_2\text{-}S)@C_s(6)\text{-}C_{82}$, the crystallographic data clearly indicate that the C_{82} cage is $C_{3v}(8)$ and *ordered* in this endohedral. However, the internal $Sc_2(\mu_2\text{-}S)$ cluster of the fullerene is disordered.[33] There are a total of six scandium and three sulfide sites in the asymmetric unit. The disordered positions of the $Sc_2(\mu_2\text{-}S)$ unit in $Sc_2(\mu_2\text{-}S)@C_{3v}(8)\text{-}C_{82}$ are shown in part C of Figure 2. The major orientation, which is the one shown in Figure 5, involves the set of atoms {Sc1, Sc2, S1}, with respective fractional occupancies of 0.60, 0.60, and 0.80. Structural parameters for this orientation are given in Table 1. A minor orientation {Sc3, Sc4, S1} was modeled that also utilizes S1 as a sulfide bridge. In this orientation both Sc3 and Sc4 refined to 0.25 fractional occupancies. The third and fourth orientations involve the sets {Sc5, Sc6, S2} and {Sc5, Sc6, S3}. The fractional occupancy of Sc5 and Sc6 are both 0.30, while the occupancies of S2 and S3 are each 0.10. Thus, the fractional occupancy of all of the scandium atom sites totaled to 2.0, and the fractional occupancies of the three sulfur atom sites was 1.0.

Computational Studies. We have computed the free energies [in the rigid rotor−harmonic oscillator (RRHO) approximation] for $Sc_2(\mu_2\text{-}S)@C_s(6)\text{-}C_{82}$, $Sc_2(\mu_2\text{-}S)@C_{3v}(8)\text{-}C_{82}$, and $Sc_2(\mu_2\text{-}S)@C_{2v}(9)\text{-}C_{82}$ isomers at different temperatures as well as their molar fractions derived from the free energy calculations. Molar fractions have been computed using two different approximations, as was done by Slanina:[34,35] (i) the RRHO approximation and (ii) a modified treatment based on experimental findings and computations that the encapsulated atoms can exercise large-amplitude motions, especially at high temperatures. This approximation is called the free, fluctuating, or floating encapsulated model (FEM).

Isomer $Sc_2(\mu_2\text{-}S)@C_{3v}(8)\text{-}C_{82}$, with a lower energy at 0 K (less than 0.2 kcal mol^{-1}), is predicted to be the most abundant product at low temperatures. The molar fraction of isomer $Sc_2(\mu_2\text{-}S)@C_s(6)\text{-}C_{82}$, which is more favored from the thermal and entropic points of view, increases at higher temperatures. Within the RRHO approximation, isomer $Sc_2(\mu_2\text{-}S)@C_s(6)\text{-}C_{82}$ is the second most abundant isomer, with a non-negligible molar fraction of around 0.3 up to 3000 K (see Figure 6). Within the FEM, however, isomer $Sc_2(\mu_2\text{-}S)@C_s(6)\text{-}C_{82}$ is predicted to be the most abundant species at $T > 100$ K (see Figure 7). Isomer $Sc_2(\mu_2\text{-}S)@C_{3v}(8)\text{-}C_{82}$ remains as the second most abundant isomer up to 3000 K, with a non-negligible molar fraction around 0.3. The molar fraction of $Sc_2(\mu_2\text{-}S)@C_{2v}(9)\text{-}C_{82}$ increases at high temperatures, but it remains as the least abundant isomer up to 3000 K within both the RRHO approximation and the FEM.

The structural parameters related to the $Sc_2(\mu_2\text{-}S)$ cluster for different orientations inside the $C_s(6)\text{-}C_{82}$ and $C_{3v}(8)\text{-}C_{82}$ cages have been computed and are shown in SI Tables SI1 and SI2, respectively. Table 1 compares the experimental and computed bond distances and angles for the $Sc_2(\mu_2\text{-}S)$ units in the two stable isomers of $Sc_2(\mu_2\text{-}S)@C_{82}$.

Table 2 contains information concerning the computed energies of the HOMO and the LUMO and the ionization potentials for $Sc_2(\mu_2\text{-}S)@C_s(6)\text{-}C_{82}$, $Sc_2(\mu_2\text{-}S)@C_{3v}(8)\text{-}C_{82}$,

dx.doi.org/10.1021/ja200289w | J. Am. Chem. Soc. 2011, 133, 6752–6760

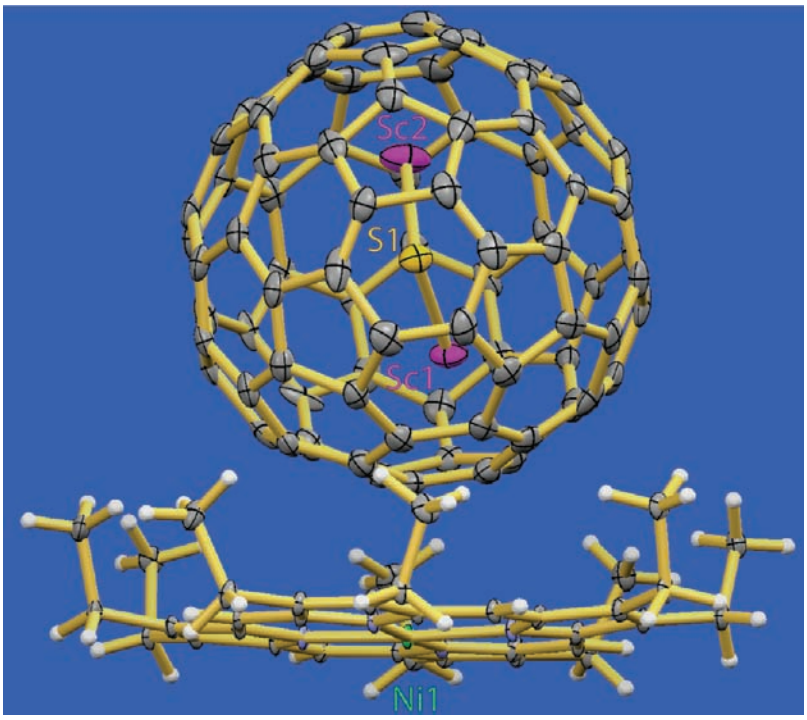

Figure 5. View of the structure $Sc_2(\mu_2\text{-}S)@C_{3v}(8)\text{-}C_{82}\cdot Ni^{II}(OEP)\cdot 2C_6H_6$ with 30% thermal contours. The three-fold axis of the fullerene is perpendicular to the page and runs through the central hexagon. Only the major site of the $Sc_2(\mu_2\text{-}S)$ unit is shown. For clarity, the benzene molecules have been omitted.

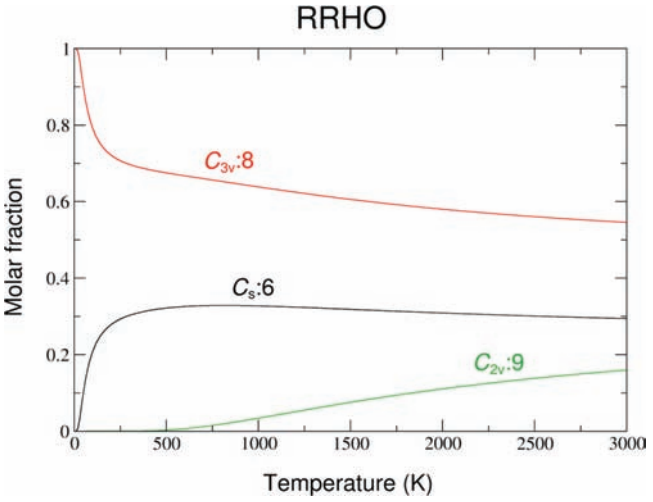

Figure 6. Predicted molar fractions with the RRHO model as a function of temperature for the three isomers of $Sc_2(\mu_2\text{-}S)@C_{82}$.

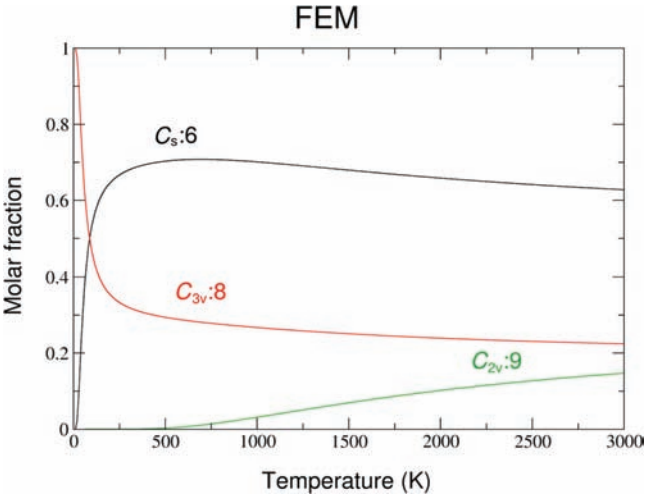

Figure 7. Predicted molar fractions with the FEM as a function of temperature for the three isomers of $Sc_2(\mu_2\text{-}S)@C_{82}$.

and $Sc_2(\mu_2\text{-}O)@C_s(6)\text{-}C_{82}$. Figure 8 shows contour diagrams of the HOMO for each of these three molecules.

Electrochemical Studies. The cyclic voltammograms (CV) of $Sc_2(\mu_2\text{-}S)@C_s(6)\text{-}C_{82}$, $Sc_2(\mu_2\text{-}S)@C_{3v}(8)\text{-}C_{82}$, and $Sc_2(\mu_2\text{-}O)@C_s(6)\text{-}C_{82}$ were recorded at a scan rate of 100 mV/s in *o*-dichlorobenzene (*o*-DCB) containing 0.05 M tetra(*n*-butyl)ammonium hexafluorophosphate, $(n\text{-}Bu_4N)(PF_6)$, as the supporting electrolyte.

As previously reported,[27] the CV of $Sc_2(\mu_2\text{-}S)@C_s(6)\text{-}C_{82}$ exhibits three reduction peaks as shown in Figure 9. The first and second reduction peaks overlap substantially with each other, whereas the third reduction peak is well defined. The reduction processes of $Sc_2(\mu_2\text{-}S)@C_{3v}(8)\text{-}C_{82}$ show a different pattern and a well-defined, fourth reduction step at a potential of −2.49 V. Moreover, while $Sc_2(\mu_2\text{-}S)@C_s(6)\text{-}C_{82}$ shows a fairly reversible first reduction, that of $Sc_2(\mu_2\text{-}S)@C_{3v}(8)\text{-}C_{82}$ is obviously irreversible. The difference in electrochemical behavior between the two isomers is also evident in the oxidative scan. While the first oxidation peak of $Sc_2(\mu_2\text{-}S)@C_{3v}(8)\text{-}C_{82}$ is shifted from the corresponding oxidation potential of $Sc_2(\mu_2\text{-}S)@C_s(6)\text{-}C_{82}$, 0.39 to 0.52 V, the second oxidation peak of of $Sc_2(\mu_2\text{-}S)@C_{3v}(8)\text{-}C_{82}$ is even more dramatically shifted relative to that of $Sc_2(\mu_2\text{-}S)@C_s(6)\text{-}C_{82}$, 0.65 to 0.96 V. These results indicate that $Sc_2(\mu_2\text{-}S)@C_s(6)\text{-}C_{82}$ and its anion are easier to be oxidized and

dx.doi.org/10.1021/ja200289w | *J. Am. Chem. Soc.* 2011, 133, 6752–6760

significant differences exist between the HOMO orbitals of two isomers.

Although the detailed relationship between the electronic structures and their electrochemical behavior is yet to be determined due to some unknown processes that occur during the oxidation and reduction processes of endohedral cluster fullerenes,[36,37] these results show that the geometrical differences between the two isomers of $Sc_2(\mu_2\text{-}S)@C_s(6)\text{-}C_{82}$ and $Sc_2(\mu_2\text{-}S)@C_{3v}(8)\text{-}C_{82}$ exert a noticeable influence on their electronic structures, especially their HOMO orbitals.

We also conducted a comparative study of the electrochemical behavior of $Sc_2(\mu_2\text{-}S)@C_s(6)\text{-}C_{82}$ and $Sc_2(\mu_2\text{-}O)@C_s(6)\text{-}C_{82}$. For the first time we investigated the influence of the nonmetal atom in the cluster on the electrochemical behavior of the endohedral cluster fullerenes with identical cage structures. As shown in Figure 9 and Table 3, the first reduction (−0.98 V) and oxidation (0.39 V) potentials of $Sc_2(\mu_2\text{-}S)@C_s(6)\text{-}C_{82}$ are very similar to those of the $Sc_2(\mu_2\text{-}O)@C_s(6)\text{-}C_{82}$ (−0.96 and 0.35 V). The differences are much smaller than those observed between the two isomers of the $Sc_2(\mu_2\text{-}S)@C_{82}$. This result indicates that $Sc_2(\mu_2\text{-}S)@C_s(6)\text{-}C_{82}$ and $Sc_2(\mu_2\text{-}O)@C_s(6)\text{-}C_{82}$ have very similar HOMO and LUMO orbitals, as shown in Figure 8 for the HOMO. This similarity is not surprising, since the two compounds have the same cage symmetry and the endohedral clusters are valence isoelectronic. Consequently, the energies of the HOMO and LUMO orbitals, as well as the H−L gaps, for these two species are very similar (see Table 2). The

Table 2. Electronic Parameters Computed in *o*-Dichlorobenzene for $Sc_2(\mu_2\text{-}X)@C_{82}$ Endofullerenes with X = S or O[a]

	$Sc_2(\mu_2\text{-}S)@C_{3v}(8)\text{-}C_{82}$	$Sc_2(\mu_2\text{-}S)@C_s(6)\text{-}C_{82}$	$Sc_2(\mu_2\text{-}O)@C_s(6)\text{-}C_{82}$
LUMO	−3.98	−4.17	−4.16
HOMO	−5.17	−5.01	−4.98
H−L gap	1.19	0.84	0.82
EA[b]	−3.61	−3.69	−3.70
IP[b]	+5.10	+4.92	+4.87
EC_{calc}[b]	1.49	1.23	1.18
EC_{exp}[c]	1.56	1.37	1.31

[a] All the energies are in electronvolts. [b] Electron affinities (EA), ionization potentials (IP), and electrochemical gaps (EC) computed in solution. [c] Experimental electrochemical gap in volts.

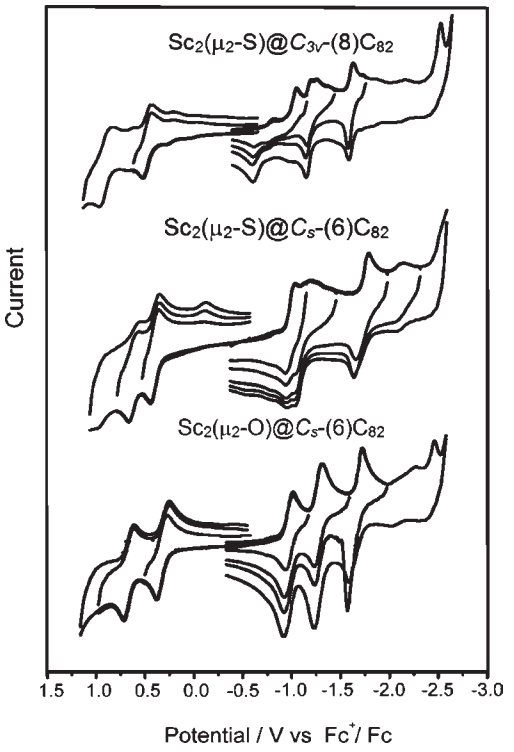

Figure 9. Cyclic voltammograms of $Sc_2(\mu_2\text{-}S)@C_{3v}(8)\text{-}C_{82}$, $Sc_2(\mu_2\text{-}S)@C_s(6)\text{-}C_{82}$, and $Sc_2(\mu_2\text{-}O)@C_s(6)\text{-}C_{82}$ in $(n\text{-}Bu_4N)(PF_6)$/o-DCB with ferrocene as the internal standard. Scan rate, 100 mV s^{-1}.

Figure 8. Contour diagrams of the HOMO orbitals for $Sc_2(\mu_2\text{-}S)@C_{3v}(8)\text{-}C_{82}$, $Sc_2(\mu_2\text{-}S)@C_s(6)\text{-}C_{82}$, and $Sc_2(\mu_2\text{-}O)@C_s(6)\text{-}C_{82}$.

Table 3. Redox Potentials of $Sc_2(\mu_2\text{-}S)@C_{3v}(8)\text{-}C_{82}$, $Sc_2(\mu_2\text{-}S)@C_s(6)\text{-}C_{82}$, and $Sc_2(\mu_2\text{-}O)@C_s(6)\text{-}C_{82}$ in $(n\text{-}Bu_4N)(PF_6)$/*o*-DCB with Ferrocene as the Internal Standard[a]

compound	$E^{0/-}$	$E^{-/2-}$	$E^{2-/3-}$	$E^{0/+}$	$E^{+/2+}$	$E^{2+/3+}$
$Sc_2(\mu_2\text{-}S)@C_{3v}(8)\text{-}C_{82}$	−1.04	−1.19	−1.63	+0.52	+0.96	
$Sc_2(\mu_2\text{-}S)@C_s(6)\text{-}C_{82}$	−0.98 (98)	−1.12 (121)	−1.73 (129)	+0.39 (88)	+0.65	+0.98
$Sc_2(\mu_2\text{-}O)@C_s(6)\text{-}C_{82}$	−0.96 (84)	−1.28 (114)	−1.74	+0.35 (121)	+0.72 (97)	

[a] Peak potential in volts. The values in parentheses are the differences between the peak potentials and the half-wave potentials in millivolts. Scan rate, 100 mV s^{-1}.

dx.doi.org/10.1021/ja200289w |J. Am. Chem. Soc. 2011, 133, 6752–6760

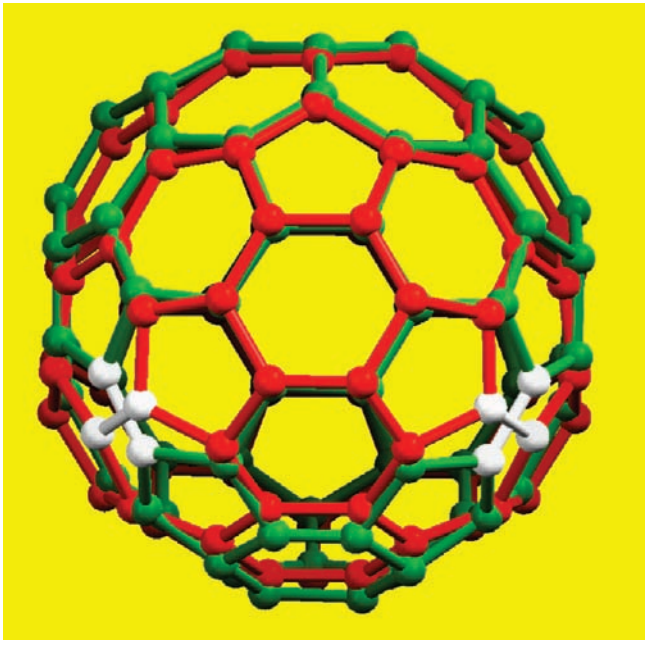

Figure 10. Structure of $C_s(6)$-C_{82}, shown in red overlaid on the structure of $C_{3v}(8)$-C_{82}, shown in green. The mirror plane present in $C_s(6)$-C_{82}, which is coincident with one of the three mirror planes in $C_{3v}(8)$-C_{82}, is perpendicular to the plane of the page. The pairs of carbon atoms that may be sequentially interconverted by Stone−Wales transformations are highlighted in white.

HOMO in $Sc_2(\mu_2\text{-}S)@C_s(6)$-$C_{82}$ (−5.01 eV) shows a somewhat lower energy than that in $Sc_2(\mu_2\text{-}O)@C_s(6)$-$C_{82}$ (−4.98 eV), in agreement with the slightly higher first oxidation potential observed in the voltammogram for $Sc_2(\mu_2\text{-}S)@C_s(6)$-$C_{82}$. The computed ionization potentials and electrochemical gaps also reproduce the experimental trends. However, as shown in Figure 9, there are the differences in the overall reduction patterns, more obvious than those observed between the two isomers of $Sc_2(\mu_2\text{-}S)@C_{82}$. This may be related to their geometrical differences. As the crystallographic data revealed, the Sc_2S cluster in the $Sc_2(\mu_2\text{-}S)@C_s(6)$-$C_{82}$ has a significantly narrower angle of 97.34 (13)°, compared to 156.6 (3)° for $Sc_2(\mu_2\text{-}O)@C_s(6)$-$C_{82}$. The Sc−S distances in $Sc_2(\mu_2\text{-}S)@C_s(6)$-$C_{82}$ are also notably larger than those of the Sc−O distances in $Sc_2(\mu_2\text{-}O)@C_s(6)$-$C_{82}$. These geometrical differences in the clusters indicate that the Sc_2S cluster is much more constrained by the cage than those of the Sc_2O cluster, which must influence the interactions between the cage and the cluster and thus their electrochemical properties.

DISCUSSION

This study has provided remarkably accurate structural data on two endohedral cluster fullerenes, $Sc_2(\mu_2\text{-}S)@C_s(6)$-$C_{82}$ and $Sc_2(\mu_2\text{-}S)@C_{3v}(8)$-$C_{82}$. The C_{82} cage is ordered in both structures. The crystallographic data for $Sc_2(\mu_2\text{-}S)@C_s(6)$-$C_{82}\cdot Ni^{II}(OEP)\cdot 2C_6H_6$ show two remarkable features: the presence of two slightly different cage sites and a *fully ordered* molecule $Sc_2(\mu_2\text{-}S)@C_s(6)$-$C_{82}$ in one of these sites. The major difference in the first feature, the presence of two different fullerene sites, is the occurrence of two orientations of the $Sc_2(\mu_2\text{-}S)$ unit at site B, while site A contains a totally ordered molecule. Fairly subtle differences between the two sites must be responsible for the change in the ordering of the internal cluster. The principle differences we have been able to identify include variation in the fullerene separation in the two sites and alteration in the proximity of the two Ni(OEP) units at the two sites as seen in Figure 3. The face-to-face porphyrins near site A have a 3.433(1) Å distance between the two nickel ions, while the corresponding Ni···Ni separation adjacent to site B is 3.497(1) Å. In regard to the fully ordered $Sc_2(\mu_2\text{-}S)@C_s(6)$-$C_{82}$ molecule in site A, it is important to realize that the interior atoms in many endohedral fullerenes suffer from disorder.[21,23,25] A prime example is found in the structure of $Er_2@C_s(6)C_{82}\cdot Co^{II}(OEP)\cdot 1.4(C_6H_6)\cdot 0.3(CHCl_3)$, where the fullerene cage is again fully ordered but the two erbium ions are distributed among 23 sites with fractional site occupancies ranging from 0.25 to 0.01.[38] Site A in $Sc_2(\mu_2\text{-}S)@C_s(6)$-$C_{82}\cdot Ni^{II}(OEP)\cdot 2C_6H_6$ is the first example where we have found a fully ordered cluster inside a fully ordered fullerene cage.

The ordered $Sc_2(\mu_2\text{-}S)$ unit at site A in $Sc_2(\mu_2\text{-}S)@C_s(6)$-$C_{82}\cdot Ni^{II}(OEP)\cdot 2C_6H_6$ has Sc−S bond distances of 2.3525(8) and 2.3902(8) Å, which are shorter than those in Sc_2S_3 (2.59 Å)[39] and in $CuScS_2$ (2.552(16) and 2.655(13) Å).[40] However, as seen in Table 1, the experimentally determined Sc−S distances for $Sc_2(\mu_2\text{-}S)@C_s(6)$-$C_{82}$ agree with the theoretically computed distances. The bond distances and angles for the $Sc_2(\mu_2\text{-}S)$ unit at site B are similar to those at site A, as shown in Table 1. It is informative to compare this $Sc_2(\mu_2\text{-}S)$ unit with the $Sc_2(\mu_2\text{-}O)$ unit in $Sc_2(\mu_2\text{-}O)@C_s(6)$-$C_{82}\cdot Ni(OEP)\cdot 1.4CH_3C_6H_5\cdot 0.6C_6H_6$.[25] In that compound both the fullerene cage and the internal $Sc_2(\mu_2\text{-}O)$ unit are disordered. As a result, a precise description of the geometry of the $Sc_2(\mu_2\text{-}O)$ unit was not forthcoming. However, at the major site with 0.38 fractional occupancy the Sc−O distances are 1.934(5) and 1.867(4) Å, and the Sc−O−Sc angle is 156.6(3)°. Thus, the Sc−S−Sc angle in $Sc_2(\mu_2\text{-}S)@C_s(6)$-$C_{82}$ appears to be narrower than the Sc−O−Sc angle in $Sc_2(\mu_2\text{-}O)@C_s(6)$-$C_{82}$, and, as expected, the Sc−S distances are longer than the Sc−O distances in these two endohedrals.

The Sc−S−Sc angles in $Sc_2(\mu_2\text{-}S)@C_s(6)$-$C_{82}$ and $Sc_2(\mu_2\text{-}S)@C_{3v}(8)$-$C_{82}$ differ. In $Sc_2(\mu_2\text{-}S)@C_s(6)$-$C_{82}$ the Sc−S−Sc angle is 113.84(3)°, whereas in the major site in $Sc_2(\mu_2\text{-}S)@C_{3v}(8)$-$C_{82}$ that angle is narrower, 97.34(13)°, and it is also narrower in two of the three minor sites. The computations also predict that the Sc−S−Sc angle will be narrower in $Sc_2(\mu_2\text{-}S)@C_{3v}(8)$-$C_{82}$ than in $Sc_2(\mu_2\text{-}S)@C_s(6)$-$C_{82}$. This is the first case where the nature and structure of the fullerene cage isomer exerts a demonstrable effect on the geometry of the cluster contained within.

As previously noted,[25,38] the $C_s(6)$-C_{82} cage possesses a band of 10 contiguous hexagons, a feature which extends to $C_{3v}(8)$-C_{82}, where there are three such bands. In both $Sc_2(\mu_2\text{-}S)@C_s(6)$-$C_{82}$ and $Sc_2(\mu_2\text{-}S)@C_{3v}(8)$-$C_{82}$, the scandium ions are located near these 10 contiguous hexagons. This arrangement of scandium ions is similar to the distribution found in the crystalline structures of related $Sc_2(\mu_2\text{-}O)@C_s(6)$-$C_{82}\cdot Ni^{II}(OEP)\cdot 1.4CH_3C_6H_5\cdot 0.6C_6H_6$, where the two scandium ions are distributed between 12 different sites, and $Er_2@C_s(6)C_{82}\cdot Co^{II}(OEP)\cdot 1.4(C_6H_6)\cdot 0.3CHCl_3$, where the two erbium ions are distributed among 23 sites along that band.

As seen in Figure 10, the experimentally determined structures of the carbon cages in $Sc_2(\mu_2\text{-}S)@C_s(6)$-$C_{82}$ and $Sc_2(\mu_2\text{-}S)@C_{3v}(8)$-$C_{82}$ have close similarity. The most significant differences lie in the orientations of the two pairs of carbon atoms shown in white. The two cage isomers may be interconverted by rotating the white carbon atoms in one by 90° to form the other isomer. This interconversion can be achieved through two successive Stone−Wales transformations, as shown in Scheme 1. The currently unobserved isomer, $Sc_2(\mu_2\text{-}S)@C_{2v}(9)$-$C_{82}$, would be an intermediate in such a process,

Scheme 1. Stone−Wales Transformation and Possible Paths for Stone−Wales Interconversion of the $Sc_2(\mu_2\text{-}S)@C_{82}$ Isomers

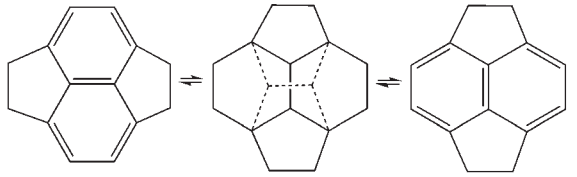

but as the data in Figures 6 and 7 show, this isomer is predicted to be less abundant than either $Sc_2(\mu_2\text{-}S)@C_s(6)\text{-}C_{82}$ or $Sc_2(\mu_2\text{-}S)@C_{3v}(8)\text{-}C_{82}$ at all temperatures.

Our computational results complement those previously reported for $Sc_2(\mu_2\text{-}O)@C_s(6)\text{-}C_{82}$. That study showed that while $Sc_2(\mu_2\text{-}O)@C_{3v}(8)\text{-}C_{82}$ was computed to be the most abundant product at low temperatures, $Sc_2(\mu_2\text{-}O)@C_s(6)\text{-}C_{82}$ becomes the most abundant species at higher temperatures due to thermal and entropic factors. For this oxide-containing endohedral the RRHO and the FEM methods produced similar results that accounted for the fact that only one isomer, $Sc_2(\mu_2\text{-}O)@C_s(6)\text{-}C_{82}$, not the two found here for the sulfide-containing endohedral, was isolated. With $Sc_2(\mu_2\text{-}S)@C_s(6)\text{-}C_{82}$ and $Sc_2(\mu_2\text{-}S)@C_{3v}(8)\text{-}C_{82}$, the RRHO and the FEM methods produce somewhat different results in regard to the question of which isomer is more stable, but this situation is consistent with the fact that two different isomers of the sulfide-containing endohedral have been isolated.

EXPERIMENTAL SECTION

X-ray Crystallography and Data Collection of $Sc_2(\mu_2\text{-}S)@C_s(6)\text{-}C_{82}\cdot Ni(OEP)\cdot 2(C_6H_6)$. Black parallelepipeds were obtained by diffusion of a benzene solution of the endohedral into a benzene solution of nickel porphyrin. The datum crystals used to obtain diffraction data for $Sc_2(\mu_2\text{-}S)@C_s(8)\text{-}C_{82}$ was large but the best specimens. A crystal with dimensions 0.90 × 0.70 × 0.15 mm was mounted on beamline 11.3.1 at the Advanced Light Source in Berkeley, CA, as described above. Diffraction data were collected using synchrotron radiation monochromated with silicon(111) to a wavelength of 0.77490 Å. An approximate full sphere of data to $2\theta = 73.2°$ was collected using 0.3° ω scans. A multiscan absorption correction was applied using the program SADABS-2008/1. A total of 159 528 reflections were collected, of which 56 317 were unique (R(int) = 0.070) and 47 544 were observed ($I > 2\sigma(I)$). The structure was solved by direct methods (SHELXS) and refined by full-matrix least-squares on F^2 (SHELXL97) using 2524 parameters and 0 restraints. All of the crystals we examined proved to be twins. The final model used the twin law −1 0 0 0 0 −1 0 −1 0 to generate an HKLF5 for refinement.[41]

The hydrogen atoms were generated geometrically and refined as riding atoms with C−H distances = 0.95−0.99 Å and $U_{iso}(H) = 1.2U_{eq}(C)$ for CH and CH_2 groups and $U_{iso}(H) = 1.5U_{eq}(C)$ for CH_3 groups. The maximum and minimum peaks in the final difference Fourier map were 2.601 and −1.603 e Å^{-3}.

Crystal data: $C_{130}H_{56}N_4NiSc_2S$, M_w = 1854.48 amu, triclinic, $P\bar{1}$, a = 14.9420(5) Å, b = 19.9180(8) Å, c = 25.3474(9) Å, α = 85.831(2)°, β = 89.630(2)°, γ = 88.845(2)°, V = 7522.2(5) Å^3, T = 100(2) K, Z = 4, $R1$ [$I > 2\sigma(I)$] = 0.0736, wR_2 (all data) = 0.1979, GOF (on F^2) = 1.055.

The crystallographic data for $Sc_2(\mu_2\text{-}S)@C_s(6)\text{-}C_{82}\cdot Ni(OEP)\cdot 2(C_6H_6)$ were initially collected at 90 K, and the crystallographic space group was identified as $P\bar{1}$ with a cell volume of 7522 Å^3. The structure was pseudomerohedrally twinned, and had $Z' = 2$. These features are indicative of an order−disorder transition. The data were recollected at 180 K, and the space group proved to be $P2_1/c$, with a cell volume equal to 7593 Å^3 and $Z' = 1$. In the latter, higher temperature structure, the Sc_2S and the C_{82} are orientationally disordered, confirming that the $Sc_2S@C_s(6)\text{-}C_{82}$ crystal undergoes a temperature dependent phase change. Due to the difficulty in modeling the disorder, we did not attempt to complete the refinement of the structure in $P2_1/c$.

X-ray Crystallography and Data Collection of $Sc_2(\mu_2\text{-}S)@C_{3v}(8)\text{-}C_{82}\cdot Ni(OEP)\cdot 2(C_6H_6)$. Black parallelepipeds were obtained by diffusion of a benzene solution of the endohedral into a benzene solution of nickel porphyrin. The datum crystal used to obtain diffraction data for $Sc_2(\mu_2\text{-}S)@C_{3v}(8)\text{-}C_{82}$ was large but the best specimen. A crystal of dimensions 0.65 × 0.65 × 0.20 mm was mounted in the 100(2) K nitrogen cold stream provided by an Oxford Cryostream low temperature apparatus on the goniometer head of a Bruker D8 diffractometer equipped with an ApexII CCD detector of beamline 11.3.1 at the Advanced Light Source in Berkeley, CA. Diffraction data were collected using synchrotron radiation monochromated with silicon(111) to a wavelength of 0.77490 Å. An approximate full sphere of data to $2\theta = 67.32°$ was collected using 0.3° ω scans. A multiscan absorption correction was applied using the program SADABS-2008/1. A total of 57 354 reflections were collected, of which 22 456 were unique (R(int) = 0.069) and 15 544 were observed ($I > 2\sigma(I)$). The structure was solved by direct methods (SHELXS) and refined by full-matrix least-squares on F^2 (SHELXL97) using 1286 parameters and 0 restraints. All of the crystals we examined proved to be twinned. The final model used the twin law 0 −1 0 −1 0 0 0 0 −1 to generate an HKLF5 for refinement.[41]

The hydrogen atoms were generated geometrically and refined as riding atoms with C−H distances = 0.95−0.99 Å and $U_{iso}(H) = 1.2U_{eq}(C)$ for CH and CH_2 groups and $U_{iso}(H) = 1.5U_{eq}(C)$ for CH_3 groups. The maximum and minimum peaks in the final difference Fourier map were 2.017 and −1.851 e Å^{-3}.

Crystal data: $C_{130}H_{56}N_4NiSc_2S$, M_w = 1854.48 amu, triclinic, $P\bar{1}$, a = 14.697(2) Å, b = 14.756(2) Å, c = 20.104(3) Å, α = 84.042(9)°, β = 84.611(9)°, γ = 61.109(8)°, V = 3791.9(9) Å^3, T = 100(2) K, Z = 2, $R1$ [$I > 2\sigma(I)$] = 0.1126, wR_2 (all data) = 0.3450, GOF (on F^2) = 1.06.

Computational Details. The calculations were carried out by using DFT methodology with the ADF 2007 package. The exchange-correlation functionals of Becke and Perdew were used. Relativistic corrections were included by means of the ZORA formalism. Slater TZP basis sets were employed to describe the valence electrons of C, S,and Sc. Frozen cores consisting of the 1s shell for C and the 1s to 2p shells for S and Sc were described by means of single Slater functions.

Electrochemistry. Cyclic voltammetry experiments were performed on a BAS 100B workstation at room temperature under the protection of a flow of argon gas. A 1 mm diameter glassy carbon rod was used as the working electrode and platinum wire and silver wire were employed as counter electrode and reference electrode respectively. The supporting electrolyte, $(n\text{-}Bu_4N)(PF_6)$ (electrochemical grade from Sigma Aldrich), was dried under reduced pressure at 340 K for 24 h and stored in a glovebox prior to use. The concentration of $(n\text{-}Bu_4N)(PF_6)$ in o-DCB solutions was 0.05 mol/L. Ferrocene was added as the internal standard before the final voltammetric cycle and all potentials are referred to the Fc/Fc^+ couple.

ASSOCIATED CONTENT

Supporting Information. Diagrams showing the numbering schemes for $Sc_2(\mu_2\text{-}S)@C_s(6)\text{-}C_{82}$ and $Sc_2(\mu_2\text{-}S)@C_{3v}(8)\text{-}C_{82}$ and computational results; X-ray crystallographic files for $Sc_2(\mu_2\text{-}S)@C_s(6)\text{-}C_{82}$ and $Sc_2(\mu_2\text{-}S)@C_{3v}(8)\text{-}C_{82}$ in CIF

format. This material is available free of charge via the Internet at http://pubs.acs.org.

AUTHOR INFORMATION

Corresponding Author
echegoyen@utep.edu; josepmaria.poblet@urv.cat; albalch@ucdavis.edu

ACKNOWLEDGMENT

We thank the National Science Foundation (Grants CHE-0716843 and Grant CHE-1011760 to A.L.B. and M.M.O., Grant DMR-0809129 to L.E., and CHE-0547988 to S.S.) for financial support; the GAANN Fellowship to B.Q.M.; and the Advanced Light Source, supported by the Director, Office of Science, Office of Basic Energy Sciences, of the U.S. Department of Energy under Contract No. DE-AC02-05CH11231, for beam time, and Dr. Simon J. Teat and Dr. Christine M. Beavers for their assistance. This work was also supported by the Spanish Ministry of Science and Innovation (Project No. CTQ2008-06549-C02-01/BQU and the Ramón y Cajal Program (ARF)) and by the DURSI of the Generalitat de Catalunya (2009SGR462 and XRQTC).

REFERENCES

(1) Kroto, H. W.; Heath, J. R.; Obrien, S. C.; Curl, R. F.; Smalley, R. E. *Nature* **1985**, *318*, 162.
(2) Heath, J. R.; Obrien, S. C.; Zhang, Q.; Liu, Y.; Curl, R. F.; Kroto, H. W.; Tittel, F. K.; Smalley, R. E. *J. Am. Chem. Soc.* **1985**, *107*, 7779.
(3) Kratschmer, W.; Lamb, L. D.; Fostiropoulos, K.; Huffman, D. R. *Nature* **1990**, *347*, 354.
(4) Akasaka, T.; Nagase, S. *Endofullerenes: A New Family of Carbon Clusters*; Kluwer: Dordrecht, 2002.
(5) Shinohara, H. *Rep. Prog. Phys.* **2000**, *63*, 843.
(6) Dunsch, L.; Yang, S. *Small* **2007**, *3*, 1298.
(7) Bolskar, R. D.; Benedetto, A. F.; Husebo, L. O.; Price, R. E.; Jackson, E. F.; Wallace, S.; Wilson, L. J.; Alford, J. M. *J. Am. Chem. Soc.* **2003**, *125*, 5471.
(8) Chaur, M. N.; Melin, F.; Ortiz, A. L.; Echegoyen, L. *Angew. Chem., Int. Ed.* **2009**, *48*, 7514.
(9) Popov, A. A.; Dunsch, L. *Chem.—Eur. J.* **2009**, *15*, 9707.
(10) Stevenson, S.; Rice, G.; Glass, T.; Harich, K.; Cromer, F.; Jordan, M. R.; Craft, J.; Hadju, E.; Bible, R.; Olmstead, M. M.; Maitra, K.; Fisher, A. J.; Balch, A. L.; Dorn, H. C. *Nature* **1999**, *401*, 55.
(11) Chaur, M. N.; Melin, F.; Ashby, J.; Elliott, B.; Kumbhar, A.; Rao, A. M.; Echegoyen, L. *Chem.—Eur. J.* **2008**, *14*, 8213.
(12) Chaur, M. N.; Melin, F.; Elliott, B.; Kumbhar, A.; Athans, A. J.; Echegoyen, L. *Chem.—Eur. J.* **2008**, *14*, 4594.
(13) Krause, M.; Ziegs, F.; Popov, A. A.; Dunsch, L. *ChemPhysChem* **2007**, *8*, 537.
(14) Nishibori, E.; Terauchi, I.; Sakata, M.; Takata, M.; Ito, Y.; Sugai, T.; Shinohara, H. *J. Phys. Chem. B* **2006**, *110*, 19215.
(15) Wang, T. S.; Chen, N.; Xiang, J. F.; Li, B.; Wu, J. Y.; Xu, W.; Jiang, L.; Tan, K.; Shu, C. Y.; Lu, X.; Wang, C. R. *J. Am. Chem. Soc.* **2009**, *131*, 16646.
(16) Shi, Z. Q.; Wu, X.; Wang, C. R.; Lu, X.; Shinohara, H. *Angew. Chem., Int. Ed.* **2006**, *45*, 2107.
(17) Valencia, R.; Rodriguez-Fortea, A.; Poblet, J. M. *J. Phys. Chem. A* **2008**, *112*, 4550.
(18) Wang, C. R.; Kai, T.; Tomiyama, T.; Yoshida, T.; Kobayashi, Y.; Nishibori, E.; Takata, M.; Sakata, M.; Shinohara, H. *Angew. Chem., Int. Ed.* **2001**, *40*, 397.
(19) Yang, H.; Lu, C. X.; Liu, Z. Y.; Jin, H. X.; Che, Y. L.; Olmstead, M. M.; Balch, A. L. *J. Am. Chem. Soc.* **2008**, *130*, 17296.
(20) Wang, T. S.; Feng, L.; Wu, J. Y.; Xu, W.; Xiang, J. F.; Tan, K.; Ma, Y. H.; Zheng, J. P.; Jiang, L.; Lu, X.; Shu, C. Y.; Wang, C. R. *J. Am. Chem. Soc.* **2010**, *132*, 16362–16364.
(21) Stevenson, S.; Mackey, M. A.; Stuart, M. A.; Phillips, J. P.; Easterling, M. L.; Chancellor, C. J.; Olmstead, M. M.; Balch, A. L. *J. Am. Chem. Soc.* **2008**, *130*, 11844.
(22) Valencia, R.; Rodriguez-Fortea, A.; Stevenson, S.; Balch, A. L.; Poblet, J. M. *Inorg. Chem.* **2009**, *48*, 5957.
(23) Mercado, B. Q.; Olmstead, M. M.; Beavers, C. M.; Easterling, M. L.; Stevenson, S.; Mackey, M. A.; Coumbe, C. E.; Phillips, J. D.; Phillips, J. P.; Poblet, J. M.; Balch, A. L. *Chem. Commun.* **2010**, *46*, 279.
(24) Fowler, P. W.; Manolopoulos, D. E. *An Atlas of Fullerenes*; Clarendon Press: Oxford, 1995.
(25) Mercado, B. Q.; Stuart, M. A.; Mackey, M. A.; Pickens, J. E.; Confait, B. S.; Stevenson, S.; Easterling, M. L.; Valencia, R.; Rodriguez-Fortea, A.; Poblet, J. M.; Olmstead, M. M.; Balch, A. L. *J. Am. Chem. Soc.* **2010**, *132*, 12098.
(26) Dunsch, L.; Yang, S. F.; Zhang, L.; Svitova, A.; Oswald, S.; Popov, A. A. *J. Am. Chem. Soc.* **2010**, *132*, 5413.
(27) Chen, N.; Chaur, M. N.; Moore, C.; Pinzón, J. R.; Valencia, R.; Rodriguez-Fortea, A.; Poblet, J. M.; Echegoyen, L. *Chem. Commun.* **2010**, *46*, 4818.
(28) Haddon, R. C. *J. Am. Chem. Soc.* **1990**, *112*, 3385.
(29) Yang, H.; Beavers, C. M.; Wang, Z. M.; Jiang, A.; Liu, Z. Y.; Jin, H. X.; Mercado, B. Q.; Olmstead, M. M.; Balch, A. L. *Angew. Chem., Int. Ed.* **2010**, *49*, 886.
(30) Lee, H. M.; Olmstead, M. M.; Iezzi, E.; Duchamp, J. C.; Dorn, H. C.; Balch, A. L. *J. Am. Chem. Soc.* **2002**, *124*, 3494.
(31) Wang, X. L.; Zuo, T. M.; Olmstead, M. M.; Duchamp, J. C.; Glass, T. E.; Cromer, F.; Balch, A. L.; Dorn, H. C. *J. Am. Chem. Soc.* **2006**, *128*, 8884.
(32) Akasaka, T.; Lu, X.; Kuga, H.; Nikawa, H.; Mizorogi, N.; Slanina, Z.; Tsuchiya, T.; Yoza, K.; Nagase, S. *Angew. Chem., Int. Ed.* **2010**, *49*, 9715.
(33) Akasaka, T.; Nagase, S.; Kobayashi, K.; Walchli, M.; Yamamoto, K.; Funasaka, H.; Kako, M.; Hoshino, T.; Erata, T. *Angew. Chem., Int. Ed.* **1997**, *36*, 1643.
(34) Slanina, Z. *Int. Rev. Phys. Chem.* **1987**, *6*, 251.
(35) Slanina, Z. *Theor. Chem. Acc.* **2007**, *117*, 315.
(36) Elliott, B.; Yu, L.; Echegoyen, L. *J. Am. Chem. Soc.* **2005**, *127*, 10885.
(37) Cardona, C. M.; Elliott, B.; Echegoyen, L. *J. Am. Chem. Soc.* **2006**, *128*, 6480.
(38) Olmstead, M. M.; de Bettencourt-Dias, A.; Stevenson, S.; Dorn, H. C.; Balch, A. L. *J. Am. Chem. Soc.* **2002**, *124*, 4172.
(39) Dismukes, J. P.; White, J. G. *Inorg. Chem.* **1964**, *3*, 1220.
(40) Dismukes, J. P.; Smith, R. T.; White, J. G. *J. Phys. Chem. Solids* **1971**, *32*, 913.
(41) Sheldrick, G. M. *Acta Crystallogr., Sect. A: Cryst. Phys., Diffr., Theor. Gen. Crystallogr.* **2008**, *64*, 112.